

Soot Microstructure in Steady and Flickering Laminar Methane/Air Diffusion Flames

JIE ZHANG[†] and CONSTANTINE M. MEGARIDIS*

Department of Mechanical Engineering, The University of Illinois at Chicago, Chicago, IL 60607

An experimental investigation is presented to identify the mechanisms responsible for the enhanced sooting behavior of strongly flickering methane/air jet diffusion flames when compared to their steady counterparts. The work extends the implementation of thermophoretic sampling in flickering, co-flow, laminar, diffusion flames. Acoustic forcing of the fuel flow rate is used to phase lock the periodic flame flicker close to the natural flicker frequency (~ 10 Hz for a burner diameter of ~ 1 cm). Soot primary sizes, determined as functions of flame coordinates, indicate that the largest soot primary units in strongly flickering methane/air flames are larger by $\sim 60\%$ than those measured in steady flames with the same mean reactant flow rates. The primary particle size measurements, when combined with the soot volume fractions reported by other investigators, indicate that soot surface areas in the flickering flame are three to four times larger than those under steady conditions. These results, along with the fact that residence times in the flickering flame are twice as long as those in the steady flame, suggest that specific soot surface growth rates under unsteady combustion conditions can be similar or even lower than those in the corresponding steady flames. Finally, the number densities of soot primaries in flickering flames are found to be higher by 30–50% than those in steady flames, thus suggesting stronger and/or extended soot inception mechanisms under flickering conditions. The combination of longer flow residence times and greater population of incipient soot particles in flickering flames appears to be primarily responsible for the higher sooting propensity of methane under laminar unsteady combustion conditions. © 1998 by The Combustion Institute

INTRODUCTION

Most completed studies of soot formation in flames have concentrated primarily on steady laminar flow configurations that allow the successful implementation of experimental techniques capable of quantifying the soot field. However, as most practical flames are turbulent and thus inherently unsteady, sooting trends for practical combustion systems cannot be readily deduced using steady-flame dynamics. As a result, recent studies [1] have begun addressing the sooting behavior of laminar flames, which are characterized by periodic unsteadiness. This behavior, known in laminar flames as flickering, results from the periodic formation of large scale vortical structures outside the flame sheet [2], which cause high rates of strain and can induce flame clip-off when hot gases rise buoyantly within the cooler ambient. Due to their cyclical temporal behavior, flickering flames bridge the gap between laminar and turbulent flames and allow the investigation of a range of residence times, temperature histories, local

stoichiometries, and strain rates, which is largely inaccessible under steady conditions.

Shaddix et al. [3] used acoustic forcing of methane fuel flow to phase lock the periodic flame flicker to the natural flame flicker frequency (~ 10 Hz for a burner of 1.1 cm diameter). They used tomographic reconstruction of extinction data obtained at 632.8 nm, laser-induced incandescence (LII) images calibrated against steady CH_4 /air extinction results, and vertically polarized scattering data ($\lambda = 283.5$ nm) to characterize the temporal and spatial development of the soot field in a moderately flickering flame. These measurements showed that the instantaneous peak soot volume fraction in forced conditions where flame tip clipping occurs is four to five times greater than that in the corresponding steady flame burning with the same mean fuel flow velocity. A Mie analysis of the soot volume fraction and scattering data in [3] suggested that enhanced sooting in flickering flames is due to larger effective mean diameters of the soot aggregates. The results reported in [3] were enhanced in a follow-up article by Shaddix and Smyth [4], who examined strongly flickering methane/air flames by using improved experimental techniques similar to

*Corresponding author.

[†]Current address: Motorola CMRC, Schaumburg, IL 60196

those implemented in [3]. The trends found in [4] for methane/air flames were very similar to those of [3]. As speculated in both studies [3, 4], the larger effective mean diameters of soot measured in the flickering CH_4/air flames may be a result of either enhanced surface growth, more intense agglomeration, or a combination of both.

A recent modeling study by Kaplan et al. [5] of the fluid dynamical, thermal, and soot fields in the CH_4/air flames analyzed in [3, 4] attributed the enhanced sooting under flickering conditions to lengthening of soot growth residence times in time-varying flow fields when compared to steady conditions. According to the computations conducted in [5], the soot enhancement in flickering flames was amplified with the extent of flicker intensity. Good agreement of the model predictions with the experimental data was demonstrated in [5].

This paper defines the morphology of soot in the steady and flickering, methane/air, co-flow, laminar, diffusion flames examined by Smyth and co-workers [3, 4]. While optical techniques provide good estimates of effective mean sizes and soot volume fractions, they have been rather limited in their ability to resolve soot aggregate microstructure. More recently, optical measurement techniques have emerged [6, 7] with the capability of producing statistical information on soot aggregate microstructure. However, these techniques require detailed multi-angle scattering measurements, which cannot be easily implemented in time-varying flames. Soot morphological data in flickering flames, when combined with effective mean size and soot volume fraction data, have the potential to identify the physical processes causing the higher sooting tendencies of methane/air flames documented under unsteady combustion conditions. The current study is the first to implement thermophoretic sampling in unsteady laminar flames, and defines the limitations of this diagnostic technique with respect to its utilization in time-varying, particle-laden flow fields. The implications of the study extend to industrial applications involving the combustion of methane-containing fuels (such as natural gas) and are relevant to enhancing radiation rates through controlled pulsation.

EXPERIMENTAL SETUP

The burner is a duplicate of that used by Smyth and co-workers [3, 4]. Laminar, methane/air non-premixed flames are operated at atmospheric pressure and are based on a co-annular burner consisting of two concentric tubes of 11.1 mm and 101.6 mm i.d., respectively. A detailed description of the burner is given elsewhere [1]. CP grade (99.7%) methane fuel flows through the inner tube, while the ventilating dry air flow is directed through the annulus between the two tubes. A steady methane flow rate of $7.5 \text{ cm}^3/\text{s}$ along with an air flow rate of $635 \text{ cm}^3/\text{s}$ produce a soot-laden flame that displays a stable shape and a luminous height of 79 mm. This flame does not release any soot to the environment (non-smoking). The reactant volume flow rates were measured using calibrated rotameters, and corresponded to standard temperature and pressure conditions.

The fuel tube at the bottom of the burner was connected to a cylindrical plenum equipped with a flexible rubber diaphragm set to vibrational motion via an attached loudspeaker [3, 4]. This burner/plenum design allowed flame operation in either the steady or the flickering mode by activating vibrational forcing of the diaphragm within the plenum. The frequency and the amplitude of the wave signal directed to the loudspeaker were controlled using a function generator and an amplifier. When the loudspeaker was driven with a sine wave at 10 Hz and 1.5 V peak-to-peak forcing amplitude, the flame was induced to flicker at the same frequency. The above fuel-forcing conditions resulted in strong flame clipping as documented in Fig. 1 (reproduced from [4]). The current study concentrates on these forcing conditions, which were termed "vigorous" in [3, 4]. The repeatability of the flickering-flame cycle was verified at the initial stages of this work using high-speed (1000 frames per second) video of flame luminosity. Even though the flickering flame exhibited increased soot concentrations with respect to the steady flame [3, 4], the soot loading remained low enough to result in no soot release under the flickering conditions investigated herein. The flames were unconfined but were operated in an enclosure that limited exposure to air currents, which can adversely affect measurements in flickering flames.

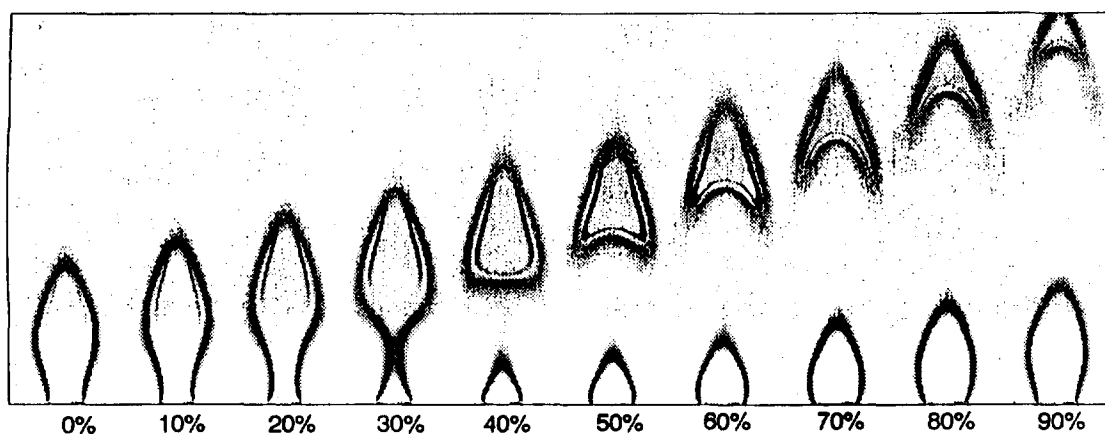


Fig. 1. OH laser-induced fluorescence and soot scattering fields in the time-varying (flickering) methane/air diffusion flame as produced by Shaddix and Smyth [4]. The fluorescence signal surrounds the scattering signal. Ten equally-spaced phase angles are shown for an acoustic excitation voltage of 1.5 V and a forcing frequency of 10 Hz, i.e., their "vigorously" flickering condition. The time interval between any two neighboring images is 10 ms.

IMPLEMENTATION OF THERMOPHORETIC SAMPLING

Thermophoretic sampling, when employed in conjunction with transmission electron microscopy (TEM), preserves the morphological state of pyrogenic soot [8] and has the demonstrated potential [9] to provide new insight to the morphology of soot aggregates produced in time-varying laminar flames. The soot morphological changes are particularly important because they define the relevant kinetic rates of soot growth and oxidation, which, in turn, determine the sooting character of a flame.

The time-varying nature of the flickering flames made the implementation of thermophoretic sampling in these flames a particularly challenging task. An electronic delay circuit was built to time the insertion of the thermophoretic probe with the sine wave input to the loudspeaker (which induces the flame flickering cycle with a constant phase angle offset). This DC circuit allowed the activation of the probe motion at well-defined instants of the flame flickering cycle, and offered good control over the duration of the probe residence time in the fully extended (soot-collecting) position. Repeatability using this device was established first with very good results. Figure 2 depicts the oscilloscope record of a sine wave (marked I) imputed to the loudspeaker—in this case 9 Hz,

~0.8 V peak-to-peak—and the signal created by the motion of the probe (marked II). The relevant time periods are indicated on that photograph and represent the parameters that can be readily modified to synchronize the motion of the probe and the flame-flickering cycle. In the specific example of Fig. 2, the thermophoretic probe motion was completed within 55 ms (insertion $t_i = 16$ ms; sample

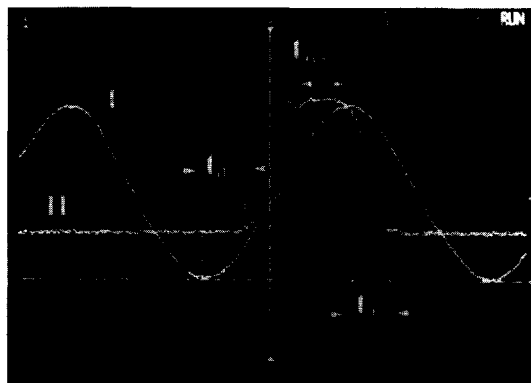


Fig. 2. Typical oscilloscope record of a sine wave (marked I) imputed to the loudspeaker (9 Hz, ~0.8 V peak-to-peak in this case) and the signal created by the motion of the thermophoretic sampling probe (marked II). The relevant time delay t_d , probe transit period t_t , and probe residence time t_{res} have been marked on the photograph. These represent the parameters that can be readily modified to synchronize the motion of the probe and the flame flickering cycle.

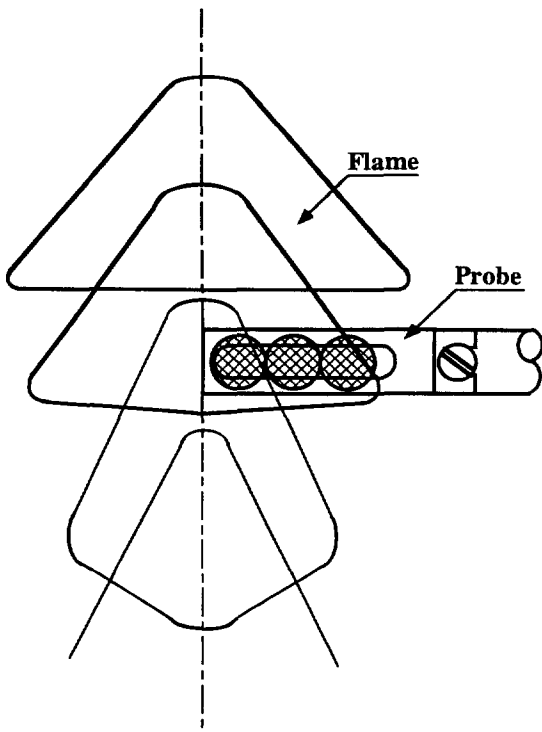


Fig. 3. Schematic depiction of the sampling procedure used in the study. The probe is inserted at a specific height above the burner and remains there until just before the base of the rising flame pocket reaches the probe. The soot aggregates contained in the rising flame pocket are captured over the length of the plate probe starting from its edge (flame axis) and gradually progressing rightward.

collection $t_{res} = 23$ ms, retraction $t_r = 16$ ms). As seen in Fig. 2, the time delay between the minimum of the sinusoidal forcing wave and the onset of the probe motion was set to $t_d = 18$ ms in this particular instance.

Typically, the thermophoretic probe motion is completed in a period of 60 ms (insertion 15 ms; sample collection 30 ms, retraction 15 ms). With a flame-forcing frequency of 10 Hz, the entire flickering cycle lasts 100 ms. Even though each thermophoretic sampling event extends over 50% of the flickering cycle, useful insight can be obtained by strategically locating the sampling probe and appropriately timing the insertion with respect to the flame flickering cycle (see Fig. 3). More specifically, a probe that is positioned over a rising flame pocket, just before its tip reaches the sampling height, would collect soot from different locations of the flame interior. To this end, the aerosol sample col-

lected on the probe would be representative of all flame regimes traversing the probe. Figures 1 and 3 show that the soot sample collected when a flamelet passes over a plate probe initially positioned above the flame tip would contain not only particles from the conical soot annulus but also from the base of the flame. In order to facilitate the interpretation of the soot morphological data when using the sampling methodology depicted in Fig. 3, the thermophoretic probe was retracted just before the lower base of the rising flamelet reached the probe. Thus, the soot sample collected at each location along the probe was dominated by particles transported in the soot annulus and passing over that location during the sampling test. Therefore, although soot samples collected in this manner give an integrated picture of both primary sizes and aggregate distribution at each location along the probe, the dominant morphology is the one representing the soot annulus, where most of the soot is contained [4].

A second methodology of soot sample collection in the flickering flame was utilized in order to improve the position correspondence between the soot collected on the probe and the flame coordinates where the sample originated from. A sequence of tests was conducted with the thermophoretic probe positioned at off-axis locations, thus collecting soot only near the probe tip as the rising flamelet "brushed" over the extended probe. This sampling methodology resulted in defining the soot morphology at the radially outermost locations of the flame during its buoyant ascent.

The soot samples collected thermophoretically using the methodologies discussed above were analyzed via transmission electron microscopy. A comparison of soot primary particle sizes between acoustically forced and steady flames with the same reactant flow rates is presented below to provide insight on their substantially different sooting behavior.

RESULTS AND DISCUSSION

Steady Flame

Soot aggregates transported in steady laminar co-annular hydrocarbon/air non-premixed flames

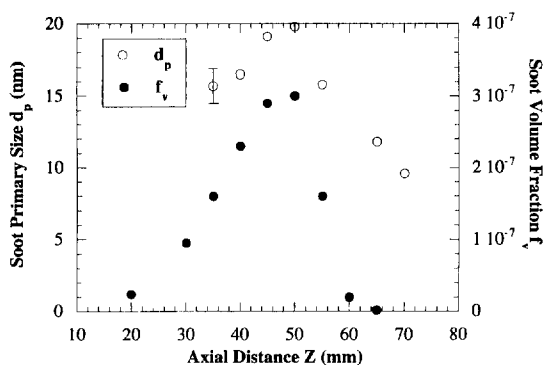


Fig. 4. Axial variation of soot size and soot volume fraction along the path coinciding with the soot annulus in the steady flame. The primary particle sizes d_p were determined by thermophoretic sampling and electron microscopy. The soot volume fractions were obtained from [4]. The error bar represents two standard deviations.

consist of primary particles of approximately spherical shape and which, for a specific location within the flame, are of nearly uniform diameter d_p [9]. However, the size of the primary particles and the degree of agglomeration (number of primary particles per aggregate) are strongly influenced by the position within the flame. Electron micrographs of the soot collected thermophoretically from various flame locations can provide (through image analysis) quantitative data on primary particle sizes.

The soot annulus at each height is defined by the radial location of maximum soot volume fraction [3, 10]. At low and intermediate heights of the steady flame, this annulus also coincides with the radial location of peak soot primary particle size, as established by the ethylene/air flame results reported in [8, 9]. A survey of d_p vs. Z along the path defining the soot annulus was performed in the steady methane/air flame by measuring a population of 120–150 primary particles at each location using a Micro-Comp high-resolution interactive morphometry station. The d_p vs. Z data along this path are presented in Fig. 4. This figure also shows the variation of soot volume fraction f_v along the same path; the values of f_v were obtained from [4]. The maximum value of d_p in Fig. 4 is about 20 nm and occurs at a height $Z = 50$ mm above the burner mouth. This axial location coincides with the height where the maximum soot volume fraction was measured along this path [4].

It is noticed in Fig. 4 that the values of f_v above $Z = 50$ mm diminish at a much faster pace than that allowed by the corresponding values of d_p . At $Z > 50$ mm, the maximum soot concentrations move near the flame axis [5] and the spatial resolution of thermophoretic sampling is compromised. To this end, the d_p vs Z variation above 50 mm should only be viewed as indicative of the overall diminishing trend of soot particle sizes at the upper portion of the flame.

Let N_p be the total number of primary particles per unit volume of the soot aerosol at a specific location Z along the path exhibiting the maximum soot volume fraction. Each location along this path is characterized by a specific primary size d_p and volume fraction f_v , both given in Fig. 4. Thus

$$N_p = \frac{6f_v}{\pi d_p^3} \quad (1)$$

It is noted that the corresponding number density of soot aggregates at each location is considerably lower than N_p . Furthermore, assuming point contact among the primaries making up each aggregate, the following expression is valid for the total surface area of particulate phase per unit volume of the soot aerosol at a specific location Z :

$$S_T = \frac{6f_v}{d_p} \quad (2)$$

Note that the above equation for S_T provides an upper bound of the actual soot surface area, because the soot aggregates consist of primary particles bridged together as a result of surface deposition [9]. The values of d_p , as determined by thermophoretic sampling (data in Fig. 4), along with the values of f_v , as determined optically by Shaddix and Smyth [4], were combined to calculate N_p and S_T from Eqs. (1) and (2). Table 1 shows some selected data for the growth stage of aggregates transported along the annular region of the steady methane/air flame. As seen from the listed values of N_p , this quantity remains practically unchanged throughout the growth region of the flame along the path line examined. The values of N_p are lower by a factor of 4 compared to those determined similarly in ethylene/air flames based on the same burner [11]. This indicates that the soot incep-

TABLE 1
Selected Data for the Path Line Exhibiting the Maximum Soot Volume Fraction in the Steady Methane/Air Flame

Z (mm)	t (ms)	d_p (nm)	f_v (cm ³ /cm ³)	v_z (cm/s)	N_p (cm ⁻³)	S_T (cm ² /cm ³)	f (g/cm ² s)	f_G (molec/cm ³ s)
30	43.0	—	9.5×10^{-8}	97.5	—	—	—	—
35	47.5	15.7	1.6×10^{-7}	101.3	7.7×10^{10}	0.60	6.9×10^{-5}	9.5×10^{17}
40	51.4	16.5	2.3×10^{-7}	103.5	9.6×10^{10}	0.82	3.8×10^{-5}	7.2×10^{17}
45	54.1	19.1	2.9×10^{-7}	105.4	8.0×10^{10}	0.92	0.7×10^{-5}	1.5×10^{17}
50	57.0	19.8	3.0×10^{-7}	106.0	7.3×10^{10}	0.90	—	—

tion rates in methane/air flames are smaller than those in their ethylene/air counterparts. The constant value of the primary particle number density in the soot growth region of the steady flame (see Table 1) also implies that primary particle coalescence (collisional growth resulting in the formation of spherical clusters) does not occur. Obviously, agglomeration and surface growth would not alter N_p . The constancy of N_p in methane/air flames agrees with previous observations on ethylene/air flames [11]. This seemingly unified trend for hydrocarbon/air co-annular flames supports the view that along the path coinciding with the soot annulus, soot inception is completed first before soot grows subsequently via surface growth. The soot formation process eventually ceases when oxidation takes over near the tip of the flame. It is noted that the values of f_v , as required for the calculation of N_p and S_T , have been obtained for the steady methane and ethylene flames (in [4] and [10], respectively) using a soot refractive index of 1.57–0.56 *i*.

The values of soot surface area listed in Table 1 (aggregates transported along the annular region) show a 50% increase from low to intermediate heights. These values of S_T are lower by one order of magnitude than those measured in similar ethylene/air flames [11]. This trend is consistent with the lower sooting tendency of methane compared to ethylene, as quantified by Shaddix and Smyth [4]. These investigators reported that the peak soot volume fraction for ethylene was 39 times larger than that for methane under steady-flame conditions.

The variation of d_p vs. Z on the soot annulus, when combined with particle velocity data, permits the calculation of the specific soot surface

growth rate f , which is defined as the mass deposition rate per unit of particulate surface area. Santoro et al. [12] demonstrated in their similar ethylene/air co-annular diffusion flames that the locus of the maximum soot volume fraction coincides with a particle path at intermediate and higher portions of the flame, thus providing a viable soot growth trajectory for the performance of such measurements. Since experimental measurements of particle velocities in the steady methane/air flame examined in this work are not available, we will assume that the coincidence of the soot annulus and a particle path line remains valid. To this end, the numerically calculated values along the particle path coinciding with the soot annulus—as provided by Kaplan et al. [5] and Kaplan [13]—were utilized in the evaluation of f along this path line. The values of the axial component of the velocity v_z are listed in Table 1 as a function of the axial location Z . It is worth noting that the axial velocities obtained from the simulations [5, 13] are close to the values determined experimentally by Richardson and Santoro [14] for a similar methane/air flame with a slightly higher fuel flow rate of 9.8 cm³/s. The dependence of any parameter on Z translates into a dependence on the residence time t of the particles (see Table 1). The Z – t correspondence of Table 1 was based on the convention that $t = 0$ at $Z = 0$ [13]. The specific surface growth rate of the primary particles is related to the soot mass density ρ_p , the axial velocity component v_z , and the Z -gradient of the primary particle diameter through

$$f = \frac{\rho_p v_z}{2} \frac{dd_p}{dZ} \quad (3)$$

The above expression for f is derived from a mass balance formulation on the surface of a primary particle under the assumption that the soot mass density remains invariant. The soot density was taken as $\rho_p = 1.86 \text{ g/cm}^3$. This value is nearly identical to 1.84 g/cm^3 , which was measured by Rossman and Smith [15] for acetylene black, and slightly larger than the value of 1.74 g/cm^3 reported by Choi et al. [16] for soot collected in the post-flame region of an acetylene/air premixed flame. The values of dd_p/dZ needed in Eq. (3) were obtained by differentiating a second order polynomial fit of the d_p - Z curve.

The values of f obtained using Eq. (3) describe the growth of the primary particles as a result of the gas-phase surface reactions. Under the assumption that the growth of each primary particle is not influenced by the presence of other primary particles in the same aggregate, the calculated value of f describes the surface growth rate of the soot aggregate as well. The values of f for the path line exhibiting the maximum soot volume fraction in the methane/air flame, as listed in Table 1, are consistently lower than those reported in [11] for similar ethylene/air flames based on the same burner. It is also seen that f decreases sharply with height, thus showing a considerable slowdown in the surface growth reaction mechanisms.

The values of f and S_T can be combined to calculate an estimate of the molecular flux f_G of the growth species causing the growth by surface deposition. If M denotes the molecular mass of the growth species and N_A is Avogadro's number, then

$$f_G = \frac{f S_T N_A}{M} \quad (4)$$

The values of f_G listed in Table 1 were determined using Eq. (4) when acetylene was assumed to be the growth species ($M = 26 \text{ g/g-mole}$). Since the values of S_T used in this calculation form an upper bound of the soot surface area, the values of f_G given by Eq. (4) overestimate the flux of the growth species. Miller et al. [17] determined net chemical production rates for acetylene in a methane/air laminar diffusion flame based on a slot burner. Typical values of the acetylene production rate

were around $10^{-5} \text{ mol/cm}^3/\text{s}$, while maximum values were roughly three times higher. The above acetylene production rates translate into net molecular production rates of $6 \times 10^{18} \text{ molec/cm}^3/\text{s}$ (typical) and $18 \times 10^{18} \text{ molec/cm}^3/\text{s}$ (peak), which are higher by 20–40 times than the rates required for the observed soot growth (Table 1). These calculations are consistent with the hypothesis that acetylene is the major growth species, but provide no direct evidence to this effect. Finally, the values of the molecular flux of the growth species in the methane/air flame (f_G in Table 1) are lower by more than one order of magnitude compared to those estimated for similar ethylene/air flames [18].

Shaddix and Smyth [4] conducted Mie calculations to produce data on particle number densities, which showed a rapid increase with height near the flame centerline and towards the top of the flame (above 50 mm). This was interpreted in [4] as a sign of significant and sustained particle inception occurring at the upper half and near the axis of the steady methane/air flame. This hypothesis was examined in the current study using thermophoretic sampling which has been shown [19] to provide insight on soot precursor microparticles. Sampling tests along the flame axis showed apparent signs of soot inception at the axial height of 50 mm. On the other hand, the soot sampled at or above 60 mm showed a microstructure typical of mature soot with no incipient particles present. Figure 5 displays the transition of soot morphology from diffuse precursor particles (bottom micrograph; $Z = 50 \text{ mm}$) to well-defined soot aggregates (top micrograph; $Z = 60 \text{ mm}$). These observations do not verify the sustained particle inception at heights above 60 mm, as suggested in [4]. Further examination of the soot volume fraction radial profiles published in [4] reveals that the soot field in this flame maintains its annular structure up to $Z = 55 \text{ mm}$, but takes a near-parabolic shape from 60 mm and above, i.e., the maximum of f_v moves near the flame axis. This dramatic shift in the character of the soot radial distribution from 55 mm to 60 mm appears to be due to an intense nucleation burst occurring on the flame axis between these heights. This hypothesis is consistent with the soot morphologies depicted in

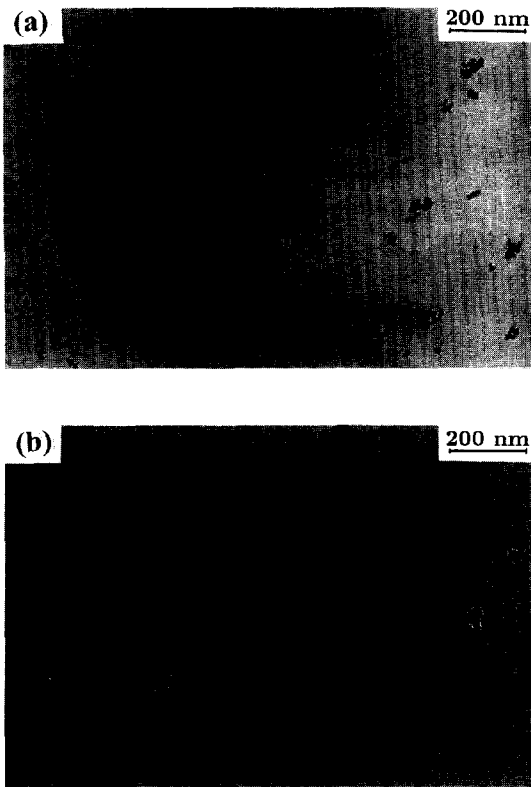


Fig. 5. Electron photomicrographs of soot collected thermophoretically from the axis of the steady methane/air flame at two heights: (a) $Z = 60$ mm, (b) $Z = 50$ mm.

Fig. 5 assuming that soot nucleation has ceased below the height of 60 mm.

Flickering Flame

An evaluation of the soot primary particle sizes within the flickering flame was conducted next. Each sampling test was monitored by high-speed video in order to establish position correspondence between probe and flame coordinates. In a typical sampling test, the probe was inserted at a fixed height in the clipped-off portion of the flickering flame, i.e., in the gap between two rising flamelets (Fig. 1). The sampling probe remained at the fully extended (soot-collecting) position until the bottom of the lower flamelet approached the probe (see Fig. 3). At that instant, the probe was retracted to avoid collection of soot from the lowest section of the luminous flame. Using this methodology, the particle morphology at every loca-

tion along the probe was dominated by the soot collected from the high-density soot annulus. However, some precursor particles were also present at most probe locations as they were collected from inner-flame regions that "brushed" over the probe after the soot annulus had already passed. The diffuse appearance of the precursor particles (which contrasted with the sharply-defined texture of mature soot) allowed a selective rejection of these particles when measuring the primary sizes corresponding to the soot annulus. This procedure was verified at the outer portions of rising flamelets by cross-comparing soot morphologies obtained when using the two different sampling methodologies described earlier.

Using the above sampling procedure, and as seen in Fig. 3, the soot aggregates contained in the rising conical flamelet are mapped over the length of the plate probe starting from its edge (flame axis) and gradually progressing rightward. Figure 6 shows a series of electron photomicrographs demonstrating soot morphology as mapped along a thermophoretic probe inserted at a height $Z = 95$ mm. Micrograph 6a corresponds to a radial location close to the flame axis, therefore it depicts soot particles collected primarily from the tip of the rising flame pocket. Some of the soot in this micrograph was collected from the inner regions of the flame when traversing over the extended probe. The diffuse precursor particles appearing in Fig. 6a were collected from the core of the rising flamelet and indicate sustained soot inception near the axis at this height. Micrographs 6b–6d correspond to increasing radial locations on the probe, and show two types of soot present: well-formed aggregates, apparently collected from the soot annulus, and precursor particles, collected from the inner fuel-rich regions of the flame. Detailed examination of a series of micrographs similar to those of Fig. 6 provided quantitative data on soot primary sizes corresponding to the soot annulus and qualitative information of the extent of soot inception as a function of flame coordinates and flickering cycle. At this stage, a simple observation of the soot aggregates seen in Fig. 6 reveals an apparent increase of primary sizes from 6a to 6d. Figure 7 depicts the primary particle sizes corresponding to the soot annulus as measured on

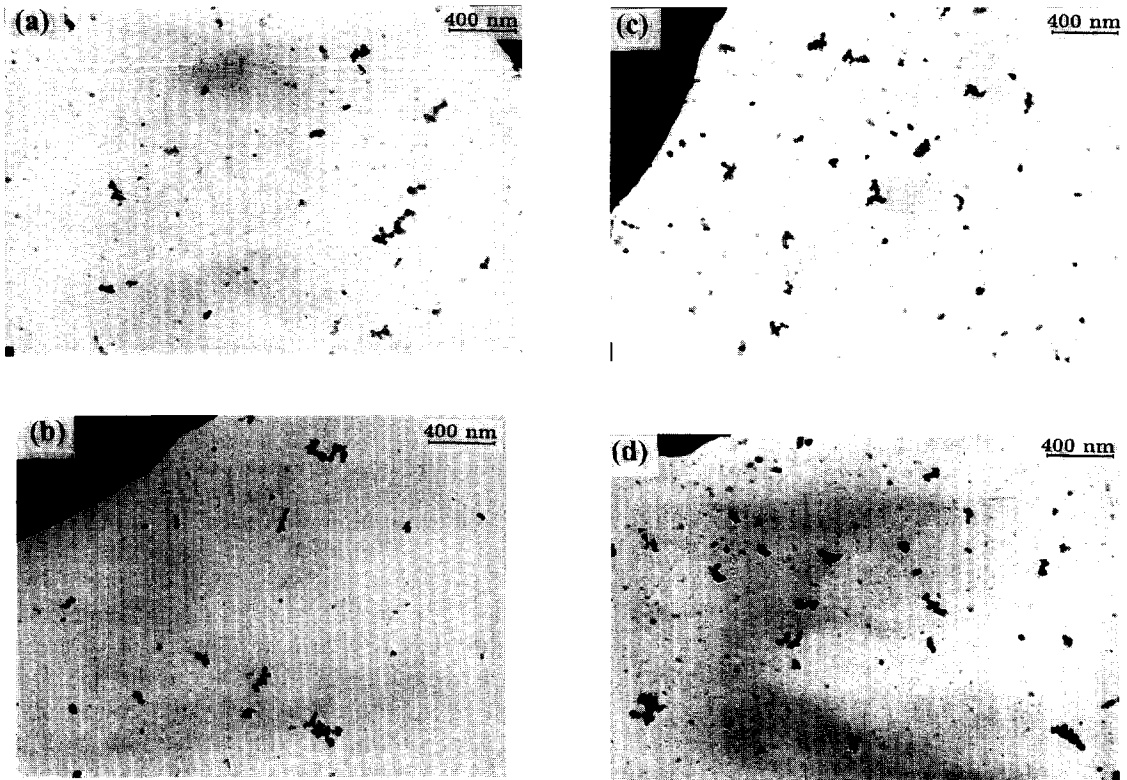


Fig. 6. Electron photomicrographs demonstrating soot morphology as mapped along a thermophoretic probe inserted at a height $Z = 95$ mm of the flickering flame. (a) $r = 2.6$ mm, (b) $r = 12.7$ mm, (c) $r = 14.4$ mm, (d) $r = 15.7$ mm. The dark corner in each of the micrographs corresponds to a section of the copper grid bar supporting the carbon film on the thermophoretic probe.

probes positioned at two different heights ($Z = 65$ and 70 mm). Values of d_p at six radial locations (labeled 1–6) are represented in each curve shown in Fig. 7. Location 1 corresponds to the flame tip, while location 6 corresponds to the base of the flame far from the symmetry axis (see markings along outline of flame image in Fig. 7). The primary particle sizes near the flame tip are smaller, probably due to ongoing oxidation. The primary sizes seen in Fig. 7 are consistently larger than those measured in the steady flame (Fig. 4), with the larger values corresponding to the radially outermost locations near the base of the flamelet.

Figure 8 presents the axial variation of soot primary sizes in the vicinity of the outer edge of the clipped-off conical flamelet as it rises buoyantly. The values of d_p seen in Fig. 8 correspond to locations 5 and 6 of Fig. 7 and reflect different phase angles of the flickering cycle. It is emphasized that the d_p vs. Z progression seen

in Fig. 8 does not reflect the same particles. The soot sizes increase up to a height of $Z \approx 80$ mm, and decrease thereafter due to oxidation. The maximum value of d_p is about 31 nm, which is larger by 57% than the maximum primary size measured in the steady flame (19.8 nm; Fig. 4).

Discussion

A comparison of the soot primary sizes measured in the time-varying methane/air diffusion flame (Figs. 7 and 8) with those in the steady flame (Fig. 4) provides insight on the origin of the higher sooting tendency of methane under flickering flame conditions. Considering that the maximum value of d_p in the flickering flame is larger by 57% than that in the steady flame, a volume ratio of about 4 is inferred for the soot primary unit. The difference in $d_{p|max}$ between steady and flickering flame conditions is apparent in Fig. 9, which shows soot aggregates with

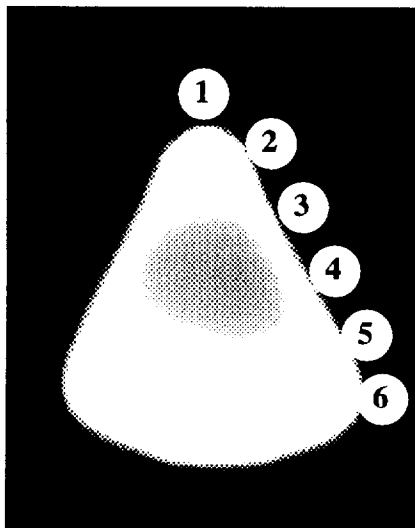
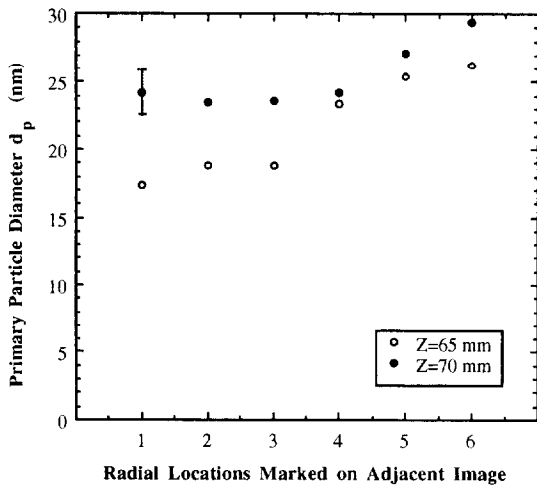


Fig. 7. Soot primary particle sizes measured at two different heights ($Z = 65$ and 70 mm) in the flickering flame using the procedure shown in Fig. 3. Values of d_p at six radial locations (labeled 1–6 in the flame image) are represented in each curve. Location 1 corresponds to the flame tip, while location 6 corresponds to the base of the flame far from the axis. The error bar represents two standard deviations.

the maximum primary size in each of the two flames. Figure 9a corresponds to the soot annulus at a height $Z = 50$ mm in the steady flame, while Fig. 9b corresponds to maximum soot sizes as obtained when a probe was positioned at a height $Z = 85$ mm in the flickering flame. It is worth noting that even though the primary sizes in 9a and 9b are distinct, no substantial differences are seen in the degree of agglomeration of the aggregates shown in these photo-

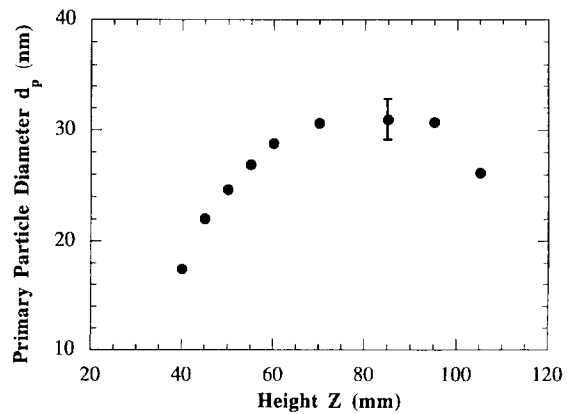


Fig. 8. Axial variation of primary particle sizes measured at locations near the base of the clipped-off flamelets and far from the centerline of the flickering flame. The error bar represents two standard deviations.

graphs. The above observations, in conjunction with the fact that peak instantaneous values of soot volume fraction are larger in the flickering flame by a factor of 5–6 [4], lead one to infer that soot surface growth mechanisms may be responsible for the higher sooting propensity of methane caused by flickering. However, because the larger soot primary sizes in the flickering flame also occur in tandem with lengthened particle growth residence times [5], additional considerations should be taken into account before definite conclusions are drawn regarding specific surface growth rates ($\text{g}/\text{cm}^2/\text{s}$) and how they compare under steady or flickering conditions.

In order to produce a comparison of specific soot surface growth rates under steady and unsteady conditions, estimates of the soot surface area are needed for the flickering flame; recall that specific surface growth rate represents the solid mass deposition rate per unit surface area of particulate phase. Our measurements provided evidence that the largest soot primary units under flickering conditions are greater by a factor of 4 (in volume) than their counterparts in the steady flame. Furthermore, according to the modeling data of Kaplan et al. [5], residence times for the soot passing through the maximum sooting region are about twice as long in the flickering flame as those predicted in the steady flame. Equation (2), along with the fact that peak soot volume fractions (and soot

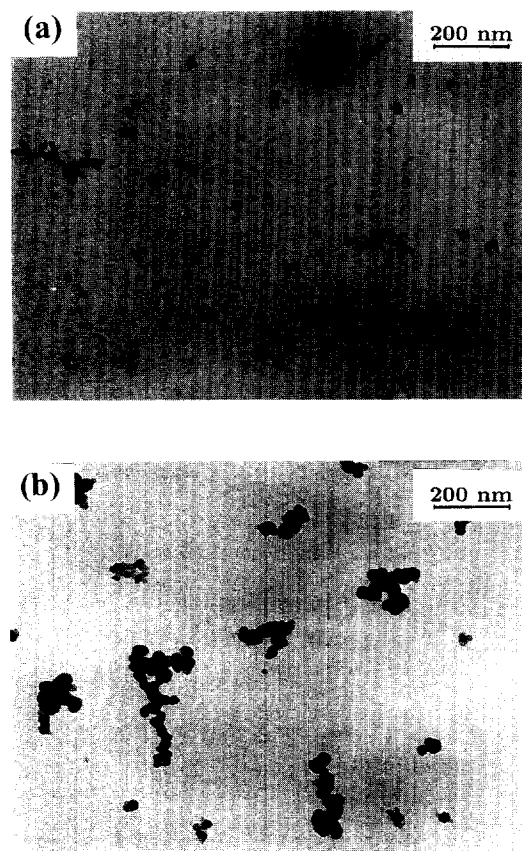


Fig. 9. Electron photomicrographs comparing soot morphology in the steady and the flickering methane/air flames. Micrograph (a) corresponds to the soot annulus ($r \sim 3.5$ mm) at a height $Z = 50$ mm in the steady flame, while micrograph (b) represents the maximum primary sizes collected on a probe positioned at $Z = 85$ mm in the flickering flame.

primary sizes) in the flickering flame are five to six (and 1.57) times larger than those in the steady flame, imply that soot surface areas in the flickering flame are three to four times larger than those under steady conditions. The simultaneous consideration of the soot mass, surface area, and residence time ratios leads to the conclusion that specific surface growth rates under unsteady combustion conditions can be similar to or even lower than those in steady flames. In addition, inspection of Eq. (1) with simultaneous consideration of the f_v and d_p ratios under flickering and steady-flame conditions implies that the number densities of the soot primaries in the flickering flame are higher by 30–50% than those in the steady flame. This

suggests stronger and/or extended soot inception mechanisms in the flickering flame. The larger population of incipient particles in the flickering flame offers additional sites for subsequent soot surface growth thus promoting higher peak values of soot volume fraction in this flame compared to its steady counterpart.

In summary, while the complex flow field in the flickering flame does not allow direct correlation of the soot morphological measurements, simple estimates based on the optical data of Shaddix and Smyth and the limited morphological data reported herein suggest that soot inception mechanisms produce a larger population of primary units under flickering conditions. Also, specific soot surface growth rates in the methane/air flickering flame are shown to be similar or even lower than those measured in the corresponding steady flame. Under enhanced soot inception and similar or weaker surface growth processes, the prolonged residence times available in the flickering flame cause the increased peak soot volume fractions and primary sizes in this flame when compared to its steady counterpart.

CONCLUSIONS

An experimental investigation has been presented to identify the mechanisms responsible for the significantly increased sooting behavior of strongly flickering methane/air flames when compared to their steady counterparts. The work extended the implementation of thermophoretic sampling—a particle sampling technique known to preserve the morphological state of pyrogenic soot—in flickering, methane/air, co-flow, laminar, diffusion flames. Acoustic forcing of the fuel flow rate was used to phase lock the periodic flame flicker close to the natural flicker frequency (~ 10 Hz). A steady methane/air flame was investigated first to establish the baseline for comparisons. Soot primary particle sizes determined in the steady flame were combined with soot volume fraction measurements and velocity data reported by other investigators to provide specific soot surface growth rates as well as soot surface areas and primary particle number densities along the path line that exhibits the maximum soot vol-

ume fraction. All of the above quantities were found to be lower than those measured previously in similar ethylene/air flames.

The reported morphological measurements indicate that the maximum soot primary particle sizes in the strongly flickering methane/air flame are larger (by ~60%) than those measured in the steady flame corresponding to the same mean reactant flow rates. The primary particle size measurements when combined with the soot volume fractions reported by other investigators (peak soot volume fractions in the flickering flame are five to six times larger than those in the steady flame) indicate that soot surface areas in the flickering flame are three to four times larger than those under steady conditions. These results, along with the fact that flow residence times in the flickering flame are twice as long as those in the steady flame, suggest that specific soot surface growth rates under unsteady combustion conditions can be similar or even lower than those in steady flames. In addition, the number densities of the soot primaries in the flickering flame were found to be higher by 30–50% than those in the steady flame, thus suggesting stronger and/or extended soot inception mechanisms in the flickering flame. The prolonged soot nucleation in the flickering flame was corroborated by experimental observations of the particle morphology. It is believed that the combination of longer flow residence times and greater population of incipient soot particles are primarily responsible for the higher sooting propensity of methane under laminar unsteady combustion conditions.

This work has been partially supported by the National Science Foundation under Grant No. CTS-9420068 and by the National Institute of Standards and Technology under Contract No. 43NANB608553. The Electron Microscopy Facility of the Research Resources Center at UIC is acknowledged for providing equipment and assistance. The authors are indebted to Dr. Kermit Smyth of NIST for helpful discussions throughout

the length of this study. The authors also thank Dr. Carolyn Kaplan of NRL for providing the modeling results relevant to this work.

REFERENCES

1. Smyth, K. C., Harrington, J. E., Johnson, E. L. and Pitts, W. M., *Combust. Flame* 95:229–239 (1993).
2. Chen, L. D., Seaba, J. P., Roquemore, W. M., and Goss, L. P., *Twenty-Second Symposium (International) on Combustion*, The Combustion Institute, Pittsburgh, 1988, pp. 677–684.
3. Shaddix, C. R., Harrington, J. E., and Smyth, K. C., *Combust. Flame* 99:723–732 (1994).
4. Shaddix, C. R., and Smyth, K. C., *Combust. Flame* 107:418–452 (1996).
5. Kaplan, C., Shaddix, C. R., and Smyth, K. C., *Combust. Flame* 106:392–405 (1996).
6. Puri, R., Richardson, T. F., Santoro, R. J., and Dobbins, R. A., *Combust. Flame* 92:320–333 (1993).
7. Farias, T. L., Carvalho, M. G., Köylü, Ü. Ö., and Faeth, G. M., *J. Heat Transfer* 117:152–159 (1995).
8. Dobbins, R. A., and Megaridis, C. M. *Langmuir* 3:254–259 (1987).
9. Megaridis, C. M., and Dobbins, R. A. *Combust. Sci. and Tech.* 71:95–109 (1990).
10. Santoro, R. J., Semerjian, H. G., and Dobbins, R. A. *Combust. Flame* 51:203–218 (1983).
11. Megaridis, C. M., and Dobbins, R. A. *Combust. Sci. and Tech.* 66:1–16 (1989).
12. Santoro, R. J., Yeh, T. T., Horvath, J. J., and Semerjian, H. G., *Combust. Sci. and Tech.* 53:89–115 (1987).
13. Kaplan, C., Personal communication, 1996.
14. Richardson, T. F., and Santoro, R. J., Personal communication, 1996.
15. Rossman, R. P., and Smith, W. R. *Ind. Eng. Chem.* 35:972–976 (1943).
16. Choi, M. Y., Mulholland, G. W., Hamins, A., and Kashiwagi, T. *Combust. Flame* 102:161–169 (1995).
17. Miller, J. H., Mallard, W. G., and Smyth, K. C. *Twenty-First Symposium (International) on Combustion*, The Combustion Institute, Pittsburgh, 1986, pp. 1057–1065.
18. Megaridis, C. M., and Dobbins, R. A. *Twenty-Second Symposium (International) on Combustion*, The Combustion Institute, Pittsburgh, 1988, pp. 353–362.
19. Dobbins, R. A., and Subramaniasivam, H., in *Soot Formation in Combustion, Mechanisms and Models* H. Bockhorn, Ed.), Springer Series in Chemical Physics 59, Springer-Verlag, Berlin, 1994, pp. 290–301.

Received 7 September 1997; accepted 4 September 1997.